Particle Rafts and Armored Droplets

Suzie Protière

Particle Rafts and Armored Droplets

Suzie Protière

Institut Jean le Rond d'Alembert, CNRS UMR 7190, Sorbonne Université, Paris, France;
email: suzie.protiere@sorbonne-universite.fr

Keywords

particle-laden interfaces, self-assembly, buoyancy, interfacial rheology, capillarity, elasticity

Abstract

Particles floating at interfaces are commonly observed in nature, as well as in industrial processes. When the particles are non-Brownian particles, large deformations of the interface are created that induce long-ranged capillary interactions and lead to the formation of particle rafts with unique characteristics. In this review we discuss recent efforts in investigating particle raft formation and the role of the rafts' own weight during dynamic clustering. Under specific conditions, these rafts can ultimately collapse and sink. When subjected to external or internal forces, the raft undergoes large deformations that test the mechanical characteristics of this interfacial composite material. It can behave as a continuous elastic sheet under compression, although its discrete nature can also trigger its fragmentation via interparticle interactions. Finally, armored droplets, drops covered by a protective shell of particles, can lose their integrity when submitted to dynamic deformations, resulting in the ejection of particles or the fracturing of the armor. Open questions to understand the properties of this material are highlighted and future research to understand the fundamental physics of particle rafts, the customization of the cluster formation, or the disassembly of this collective material is suggested.

1. INTRODUCTION

A raft is known as the most primitive structure used for transportation over water. It usually consists of a flat assembly of buoyant materials that keep it afloat. Such floating structures can also self-organize at the interface between two fluids of different densities ρ_1 and ρ_2 (with $\rho_1 > \rho_2$) via capillary interactions and are then called particle rafts. The study of such particle rafts seems particularly relevant to take on some of the challenges imposed by the numerous ecological crises we are currently living through. Shade balls have been dispersed at the surface of lakes all over the world to form large rafts protecting lakes from evaporation due to the increasing temperatures (Lehmann et al. 2019). Giant plastic garbage patches have gradually formed as a result of marine pollution in every ocean on the planet. They consist of fragments of all sizes of plastic debris gathered into clusters by ocean currents and trapped in vortices, which thus keep accumulating and damage ecosystems (Cózar et al. 2014). When rafts are formed of dense particles ρ_{part} (with $\rho_{\text{part}} > \rho_1 > \rho_2$), they can also be used to clean up oil spills. In this case, the raft undergoes strong deformations and sinks while encapsulating the lighter fluid in the process (Abkarian et al. 2013). For industrial purposes, and at a smaller scale, colloidal particles trapped at a liquid interface also self-assemble into a 2D cluster and are commonly used nowadays to stabilize emulsions (Pickering 1907, Binks & Horozov 2006).

The capillary attraction leading to the formation of such rafts occurs when the shape of an interface is perturbed by several objects. To minimize the surface energy, the deformations overlap and create an attractive force between the objects. They then self-assemble into a 2D monolayer at the interface. Understanding the formation of aggregates or clusters has always been a challenge, and the 2D visualization imposed by the liquid interface makes the process easier by allowing researchers to use statistical tools to quantify the formation of aggregates in general, as well as to investigate the role of capillary forces, which is in itself a topic of interest. Moreover, the long-ranged attraction is linked to the capillary length $\ell_c = \sqrt{\gamma_{12}/\Delta\rho g}$, with γ_{12} the interfacial tension and $\Delta\rho = (\rho_1 - \rho_2)$ the density difference between the two fluids. Short-ranged attractive or repulsive forces (Van der Waals or electromagnetic interactions) can also play an important role in the dynamics near the particle clustering (Domìnguez et al. 2010). Interestingly, this long-ranged capillary clustering via interface deformation has also been compared to 2D gravitational attraction. It was found that a tunable cutoff length related to the value of ℓ_c influences the collapse or limits the clustering of the particles (Bleibel et al. 2011).

The interface deformations can be due to the wetting properties or the shape of the particles (Danov et al. 2005, Loudet et al. 2005); however, in this review, we focus on rafts that are composed of large particles that have self-assembled via the deformation of the interface created by their weight. Such particle rafts are also called granular rafts when the particle size R_{part} is comparable to the capillary length ℓ_c. In this case, the capillary interactions cannot be controlled by the particle's shape alone, and the raft can undergo large deformations in order to sustain its weight.

The properties of particle rafts are controlled by capillary interactions during the aggregation process. The superhydrophobicity of fire ants allows them to form strong cohesive rafts that can self-heal to protect the colony (Mlot et al. 2011) (**Figure 1*a***). Mosquito eggs or whirligig beetles form long chains (**Figure 1*b***) when interacting due to their ellipsoidal shape (Loudet & Pouligny 2011, Voise et al. 2011). Particles can be designed in order to create organized structures (Bowden et al. 1997). An external field can also guide particles during their capillary self-assembly. Liu et al. (2018) discussed the role of surface curvature in order to move particles along curvature gradients: Cylindrical particles migrate along curvature gradient lines formed by a liquid interface pinned to a micropost and orient the colloid's position (**Figure 1*c***). At the millimeter scale, the dynamic self-assembly of objects has also been investigated in a series of experiments involving the formation of patterns of floating magnetic disks subjected to a magnetic field (**Figure 1*d***) (Grzybowski et al.

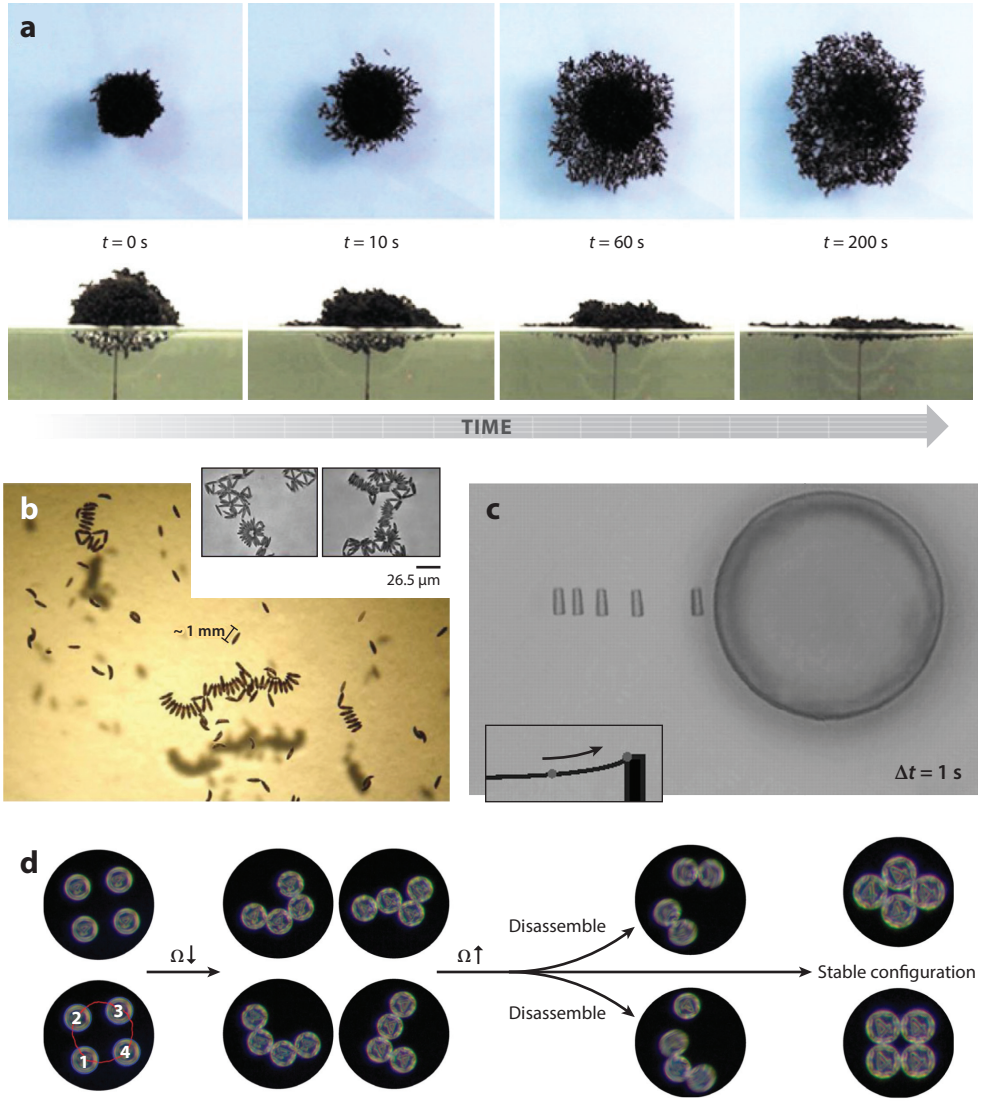

Figure 1

Examples of particle rafts found in nature or formed via capillary-driven self-assembly. (*a*) Top and side views of the construction of a raft consisting of ~3,000 ants. The ants redistribute themselves until reaching equilibrium. (*b*) Mosquito egg rafts floating on water (size: 1 mm). The eggs aggregate at the interface similarly to ellipsoidal micrometer-sized particles. (*c*) Cylindrical particles' orientation is controlled by a curved interface formed by its pinning to a micropost. (*d*) Spinning of four circular magnetic objects that self-assemble at the air–water interface. Depending on the spinning speed Ω, the particles will assemble, disassemble, or reconfigure. Panels adapted with permission from (*a*) Mlot et al. (2011), copyright 2011 National Academy of Sciences; (*b*) Loudet & Pouligny (2011), copyright 2011 EDP Sciences, SIF, and Springer-Verlag; (*c*) Cavallaro et al. (2011), copyright 2011 National Academy of Sciences; and (*d*) Wang et al. (2017) (CC BY-NC 4.0).

2000, Wang et al. 2017) and more recently with experiments in which the shapes of floating objects change due to temperature changes or light actuation (Hu et al. 2020, Vandewalle et al. 2020). These promising studies show that a raft's overall structure can be customized via a programmable self-assembly of the individual objects.

Finally, a particularly interesting feature of particle rafts is that they behave as a single entity but also exhibit granular characteristics due to their discrete assembly. The rheology and mechanics of these interfaces have been the subject of extensive investigations in the past decade. In particular, owing to this dual nature, various interfacial phenomena such as buckling or fracturing can be observed in particle-laden interfaces.

2. FORMATION OF A PARTICLE RAFT

A fluid–fluid interface is created when a junction is formed between two immiscible fluids: a lower phase denoted as phase 1 and an upper phase denoted as phase 2 throughout this review. When objects are sprinkled at such an interface, they start to interact via capillary forces. These forces have been studied for over 70 years for two identical objects. In this section, we investigate the aggregation of multiple objects at a liquid interface. We first briefly introduce the different types of capillary forces and in particular the interaction of noncolloidal particles, which is the focus this review. We then briefly recall the dynamics of interaction between two identical objects at a liquid interface and detail the forces at play. Finally we describe how two deformable nonidentical bodies interact, which then enables us to understand the global dynamics of particles interacting on a liquid interface.

2.1. Capillary Forces Between Two Particles: From Colloids to Large Objects

Particles trapped at a liquid interface interact with each other via capillary forces (**Figure 2**). These forces can be divided into two categories (Kralchevsky & Denkov 2001): normal forces and lateral capillary forces. Normal forces bind objects together by a capillary bridge: either a liquid bridge in a gas or a gas bridge in a liquid. This attractive force is produced by a pressure drop across the curved interface, as well as by the surface tension exerted along the contact line. It is directed normally to the plane of the contact line (**Figure 2*a***). This force is at play in sandcastle-building (Hornbaker et al. 1997), the dispersion of pigments, or the adhesion of powders on surfaces, for

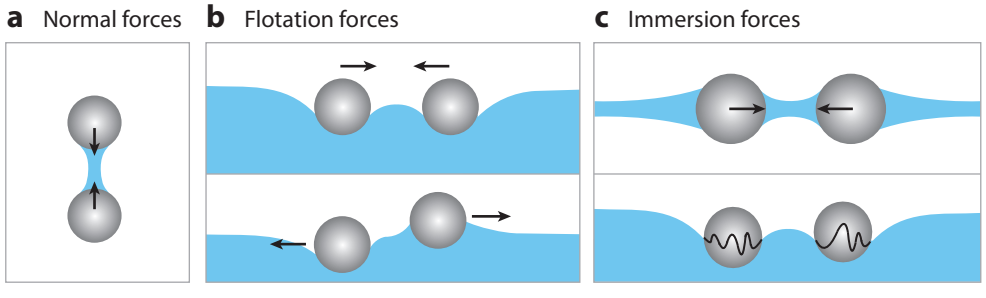

Figure 2

Capillary forces between two objects. (*a*) Normal capillary forces. The liquid is represented in blue, while the surrounding fluid is white. A capillary bridge connects the two interacting particles, leading to an attractive normal force. (*b*) Flotation forces are caused by the weight of the object, leading to a lateral force. If the two objects deflect the interface in the same direction, the force is attractive; otherwise it is repulsive. (*c*) Immersion forces can arise in different situations: due to the confinement of colloidal particles inside a liquid layer that decays at infinity (*top*) or to the undulation of the contact line induced by the particles' surface properties (*bottom*). Figure adapted from Lagarde (2020) with permission; copyright 2020 the author.

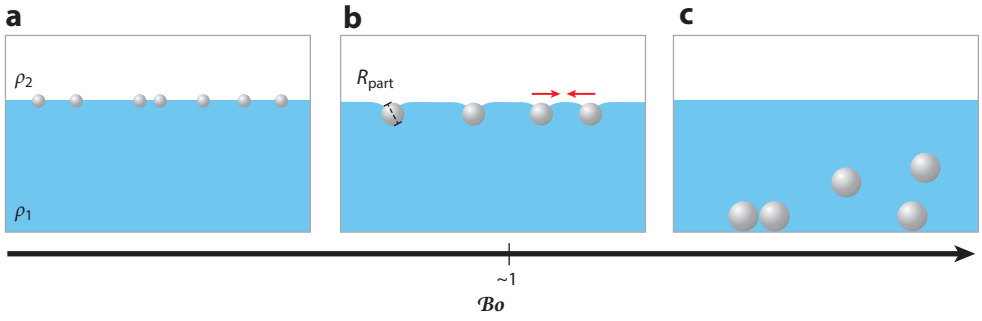

Figure 3

Particles interacting with a liquid interface, with $\rho_1 \leq \rho_{part}$. (*a*) For Bond number $\mathcal{B}o \ll 1$, perfectly smooth spheres will get trapped at the interface without creating any distortion. (*b*) For $\mathcal{B}o \sim 1$, the particle's weight creates a deformation of the interface. Two such particles will undergo an attractive capillary force and move toward each other in order to minimize surface energy. Red arrows indicate the particles' capillary attraction at the interface. (*c*) For $\mathcal{B}o \gg 1$, the particles will sink.

example (Kralchevsky & Nagayama 2001). The objects can also distort the liquid interface once trapped and are then set in motion so as to minimize the interfacial area. This creates a second category of capillary forces called lateral forces.

When the deformation of the interface is due to a perturbation of the contact line, we call the forces of interaction lateral immersion forces (Kralchevsky & Nagayama 1994) (**Figure 2*c***). This phenomenon is mostly observed at the colloidal scale where Brownian motion is overcome by capillary forces, which can appear when the particles are confined inside a liquid layer that decays either at infinity or at a finite distance. When they float at the surface of a liquid, the force is produced by an irregular contact line due to the surface roughness or chemical inhomogeneities (Stamou et al. 2000). For perfectly smooth colloidal spheres at equilibrium wetting conditions, they will leave the interface around them unperturbed (**Figure 3*a***). In this situation, the Bond number $\mathcal{B}o = (R_{part}/\ell_c)^2$, the dimensionless number comparing capillary and gravity forces, is much smaller than 1. Moreover, nonspherical shapes can also create distortion fields around them which play a central role in particle interactions that we will not detail here.

In this review, we focus on lateral capillary forces observed when the shape of an interface is perturbed by the weight of the objects (**Figure 3*b***). The interface is then pulled down locally. In this case, the Bond number $\mathcal{B}o$ is close to 1. We call this force a lateral flotation force, and it creates an interaction between objects at a fluid interface (**Figure 2*b***). At an air–water interface, the deformation can be directed downward if the particle is denser than water or upward if the object is considered lighter (a bubble, for instance). For spherical particles, the deformation is axisymmetric (the bead acts as a monopole). Of course, if the particle's weight exceeds its buoyancy, it will not remain at the interface as it will sink (**Figure 3*c***).

We wish to draw the reader's attention to the fact that the wettability of the particles (and thus the contact angle) can also play an important role [reported at length by Kralchevsky & Nagayama (1994)], but since we are discussing particle rafts, where the weight of the particles is primarily responsible for the clustering of the particles, we have decided, for clarity reasons, not to discuss it further in this review.

Bond number: dimensionless number comparing capillary and gravity forces, $\mathcal{B}o = (R_{part}/\ell_c)^2$

2.2. Dynamics of Two Particles

In this section we discuss the capillary interaction of two identical objects at a liquid interface. We first describe the forces at play and then detail the hydrodynamic interaction.

2.2.1. The Cheerios effect. We focus here on the interaction of objects at a liquid interface for which gravity plays an important role. This interaction is also commonly called the Cheerios effect (Vella & Mahadevan 2005), after the clustering of cereal observed when one pours cereal into a bowl of milk. The particle's radius R_{part} is larger than 10 μm and its weight or buoyancy cannot be neglected (**Figure 3*b***).

The attractive force between two bubbles floating on a fluid was first studied by Nicolson (1949), who proposed a model using a linear superposition approximation of the interface deformations to describe the force of interaction between the bubbles. Since then, this approximation has been used in a variety of works: for the interaction between parallel infinite cylinders (Gifford & Scriven 1971, Allain & Cloitre 1993) or particles floating on a liquid (Chan et al. 1981, Kralchevsky et al. 1992, Paunov et al. 1993, Fournier & Galatola 2002, Vassileva et al. 2005). These works have led to an analytical solution for the capillary force between two particles. However, this expression cannot be used directly, as it depends on the position of the contact line around each particle, a physical quantity unknown a priori. The calculation by Vella & Mahadevan (2005) considers the vertical equilibrium of a single particle at an interface (Binks & Horozov 2006) and then adds the second particle to calculate an interface energy.

The shape of the interface between two objects results from how the particles deform the interface: their weight, their wettability, and the induced buoyancy. These parameters can be taken into account with dimensionless numbers: the Bond number $\mathcal{B}o$, the particle–liquid density ratio $\mathcal{D} = \rho_{\text{part}}/\rho_1$, and $\Sigma = \frac{2\mathcal{D}-1}{3} - \frac{1}{2}\cos\theta + \frac{1}{6}\cos^3\theta$. In the case of small spheres ($R_{\text{part}} \ll \ell_c$) where the shape of the interface is isotropic around each bead and its deformations are small, the calculation leads to an energy of interaction equal to the product between the effective weight of one particle, $F_g + F_{\text{buoy}} = 2\pi\gamma_{12}R_{\text{part}}\mathcal{B}o\Sigma$, and the vertical deformation created by the other:

$$E(r) = 2\pi\gamma_{12}R_{\text{part}}\mathcal{B}o\Sigma\left[-\mathcal{B}o\Sigma R_{\text{part}}K_0(r/\ell_c)\right], \qquad 1.$$

with K_i the modified Bessel function of the second kind of order i. By deriving Equation 1 with respect to r (the radial coordinate), we obtain the final expression for the horizontal force between two identical particles at a fluid–air interface:

$$F_{\text{cap}}(r) = 2\pi\gamma_{12}R_{\text{part}}\mathcal{B}o^{5/2}\Sigma^2K_1(r/\ell_c). \qquad 2.$$

2.2.2. The hydrodynamics of two identical spheres at a fluid–liquid interface. At this scale, this capillary force F_{cap} is counterbalanced by a drag around each particle (**Figure 4*a***). We assume that the particles can be slowed down by the upper phase of density ρ_2. The particle's inertia can also be neglected: The particle moves in a creeping flow once attached to the interface. We thus have the Reynolds number $\mathcal{R}e = \rho V R_{\text{part}}/\mu_2 \ll 1$, with μ_2 the characteristic viscosity of the upper fluid and V the characteristic particle velocity. The viscous stresses compared with surface tension are negligible, which gives the capillary number $\mathcal{C}a = \mu_2 V/\gamma_{12} \ll 1$. The drag force acting on a particle F_{drag} can be expressed as a Stokes drag corrected by a mobility function G for two spheres in a single phase, in order to take into account the drainage of the liquid between the particles as they get closer:

$$F_{\text{drag}} = 6\pi\mu_2 R_{\text{part}}kVG^{-1}\frac{L}{R_{\text{part}}}, \qquad 3.$$

where L is the distance between the centers of the two spheres. The term k accounts for the fact that the particles are immersed in two phases (Dani et al. 2015) and depend on the contact angle of the spheres and the phases' viscosities (Danov et al. 1995, 2000; Pozrikidis 2007). The mobility function G was tabulated by Batchelor (1976) and Batchelor & Green (1972) and can be approximated by various interpolation formulas (Vassileva et al. 2006, Boneva et al. 2007). Since

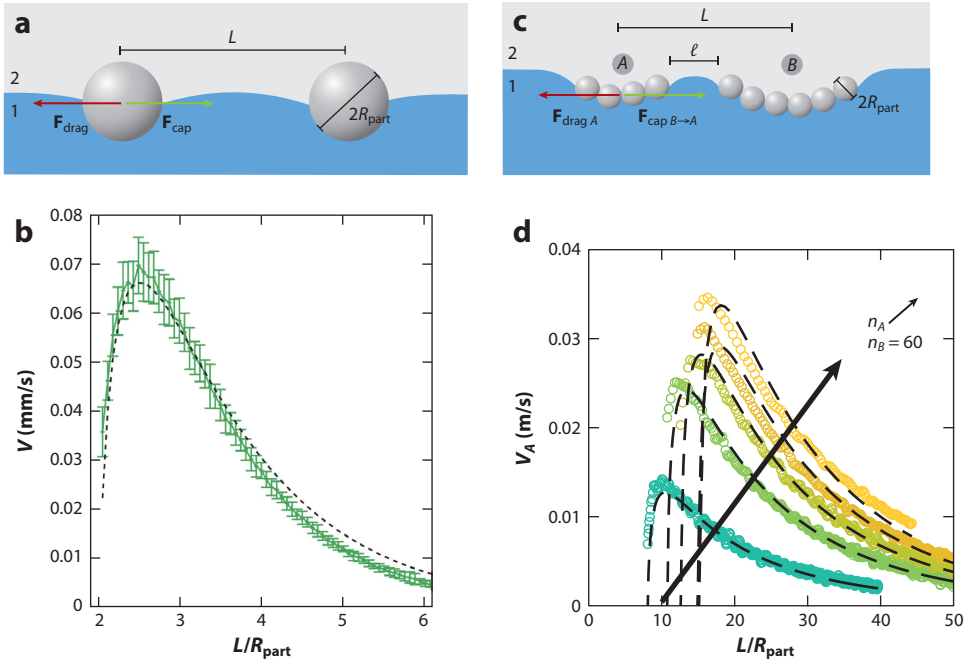

Figure 4

The kinematics of two identical spheres and two particle rafts. (*a*) The interaction between two identical spheres, both subjected to a capillary attraction and a viscous drag. (*b*) Speed V of the particle as a function of the distance between the two particles, L/R_{part}. The dashed line corresponds to Equation 4. (*c*) The interaction between two rafts A and B made of n_A and n_B particles, respectively. (*d*) Speed of the raft of increasing size ($n_A = 1, 5, 10, 20, 40$) attracted to a raft of fixed size ($n_B = 60$) as a function of the nondimensional distance L/R_{part}. Dashed lines correspond to the velocity found using Equations 5 and 6. Panels adapted with permission from (*a*,*c*) Lagarde (2020), copyright 2020 the author; (*b*) Dalbe et al. (2011), copyright 2011 American Physical Society; and (*d*) Lagarde et al. (2019), copyright 2019 Royal Society of Chemistry.

$\mathcal{R}e \ll 1$, there is no inertia and the equilibrium of forces (Equations 2 and 3) gives an expression for the velocity of one particle separated by a distance L from a second identical particle:

$$V = \frac{\gamma_{12}\mathcal{B}o^{5/2}\Sigma^2}{3\mu_2 k} G\left(\frac{L}{R_{part}}\right) K_1\left(\frac{L}{\ell_c}\right). \quad 4.$$

This model is then verified experimentally by recording the aggregation dynamics of two identical spheres and measuring their velocities. We first observe an increase in velocity as the particles get closer until a maximum is reached. From this point onward, the drainage of the liquid separating the two spheres will make the velocity decrease rapidly until contact is reached (**Figure 4*b***). The fitting parameter k has been discussed in different experimental cases by varying the wettability and the viscosity of the two fluids (Vassileva et al. 2006, Dalbe et al. 2011, Dani et al. 2015).

2.3. Clustering Dynamics of Large Objects

The models and experiments we have discussed so far concern the interactions of two identical particles. To understand the formation of particle rafts, we now detail the interactions of larger clusters.

2.3.1. Interaction of two particle rafts. Once two spherical particles are in contact they form a new aggregate at the interface. These 2D structures interact with other large clusters. These assemblies of particles have been considered as single entities in order to investigate the role of cluster dimensions on their interactions. Indeed, the capillary force experienced by each raft can strongly depend on its size and on the external interfacial deformation.

Lagarde et al. (2019) focused on the interaction of such large objects, where dense millimeter-sized beads act as monopoles. Such 2D structures are flexible and exhibit high deformations due to both their weight and their geometrical extension. They describe the capillary forces generated by each raft, as well as the drag due to their individual motion (**Figure 4*c***). Because the deformation around a particle raft strongly depends on its size, the capillary interaction can exceed by several orders of magnitude the forces created by individual beads, with a very strong dependence on the number of particles (**Figure 4*d***). The model for a two-particle interaction can be generalized to the interaction of two particle rafts. The dependence of the drag and the capillary force experienced by a raft is then quantified depending on both its size (number of particles n) and the size of the other interacting raft:

$$F_{\mathrm{cap}B\to A} = n_A n_B F_{\mathrm{cap}}, \quad 5.$$

$$F_{\mathrm{drag}A} = \sqrt{n_A} F_{\mathrm{drag}}, \quad 6.$$

with n_A and n_B the number of particles in rafts A and B, respectively.

We must note that the model used here is based in part on the assumption that the deformations due to the weight remain small when compared to the capillary length ℓ_c. However, this is not always the case, as a granular raft's vertical deformation can reach $\ell_c/2$ and its lateral extension can be close to ℓ_c. This could explain the disagreement between the experimental and theoretical speeds measured for large clusters (yellow curves in **Figure 4*d***).

2.3.2. Clustering. The next step is to explore the aggregation of a random number of particle rafts to understand the clustering dynamics and the formation of such monolayers of grains. This clustering has been studied extensively for colloidal particles, where the motion is completely controlled by Brownian thermal agitation. Universal laws that characterize aggregating systems have been theorized (Leyvraz 2003), from the fragmentation or merging of asteroids due to the collisions of planets (Lee 2000) to the formation of a fog resulting from the suspension of micrometer-sized water droplets that coalesce and break apart (Friedlander et al. 2000). In all these physical systems, statistical tools are used to describe the ordering arising from the interaction of these individual objects (Weitz & Lin 1986, Lin et al. 1989).

3. THE STABILITY OF A PARTICLE RAFT

We have discussed how particles, once placed at a liquid interface, attract each other, via a capillary force F_{cap}, to minimize the deformation of the interface. These interactions lead to the formation of a monolayer of grains. We now wish to focus on the stable equilibrium state of this new entity. At equilibrium, one object is straddling the interface between the two fluids. When an object is destabilized, it becomes out of equilibrium and sinks. First, we discuss the stability of one object, before turning to how the interaction of two or several objects at a fluid interface can lead to a collective sinking instability of the raft. Finally, we discuss how this new structure consisting of an assembly of distinct objects becomes out of equilibrium and describe various collapsing processes.

3.1. Individual Particles

Schoolchildren may recall that when an object is placed at the surface of a liquid, Archimedes' principle determines whether the object will float or sink: The upward force on a body immersed or floating in a liquid is equal to the weight of liquid displaced by that body. Surprisingly, only recently has this principle been generalized to incorporate surface tension (Keller 1998), which plays an important role when the object's size is comparable to the length of the deformed interface, ℓ_c. In this case, one has to take into account the liquid displaced not only by the object's weight but also by its meniscus. Objects with densities ρ_{part} significantly larger than that of a liquid will only float for $R_{part} \ll \ell_c$ (**Figure 3*b***). In the previous section, we introduced the parameter $\mathcal{D}$, which corresponds to a density ratio and is used, along with $\mathcal{B}o$, to characterize the deformation of a fluid interface. In his review, Vella (2015) suggested considering this same parameter $\mathcal{D}$ when evaluating whether an object can float in equilibrium at an interface and found that, to determine an object's ability to float, one has to consider a variety of its characteristics: its density and size, which directly affect its floatability, but also its shape and surface properties, which impact the length of the contact line and thus play a role in the equilibrium state of these small objects at a fluid interface.

3.2. Two Particles

The equilibrium conditions under which an object floats at an interface have been the topic of studies since Archimedes' principle. However, when several objects interact at the surface of a liquid, this compromises their equilibrium and the newly formed object may eventually sink. This topic has been investigated only recently. Indeed, since the floatability of an object is related to the shape of its contact line, when objects interact at a fluid surface during the formation of a particle raft, the shape of the contact line may vary and change the objects' load-bearing capacity (Vella et al. 2006b). In particular, Cooray et al. (2017) have found that flotation capacities can be enhanced or reduced depending on the size of and the distance between particles, as the hydrostatic pressure is in competition with the surface tension when the meniscus changes shape at the contact line during the interaction of the two objects. This may have some impact on the raft's formation.

3.3. Assembly of Particles at an Interface: Collective Stability

Once the stability of a couple of particles is understood, the next step consists in adding progressively more particles to increase the size of the cluster and see if the newly formed particle raft will stay afloat. It is difficult to predict the general conditions of stability of a raft: Although individual grains may produce deformations of the interface, when these deformations overlap and form this structure, they produce a global deformation that may not be predicted only by summing up the local capillary interactions. We therefore consider the raft as a new composite material made of the particles and the liquid, thus obtaining a scaled density ratio $\mathcal{D}$, where the load ρ_{part} at the scale of the raft thickness R_{part} is compared to the buoyancy $\Delta\rho$ at the scale of the capillary length ℓ_c:

$$\mathcal{D} = \frac{\rho_{part}}{\Delta\rho}\frac{R_{part}}{\ell_c}. \qquad 7.$$

With this parameter in mind, we can test the stability of a raft for different particle and liquid characteristics. Thus far, we have considered the case where the upper fluid is a gas of negligible density, but Protière et al. (2017) studied the stability of an axisymmetric raft formed of dense particles at an oil–water interface. In this case, the capillary attraction is long ranged, $\ell_c \approx$ 10 mm, and more importantly, the raft can undergo strong deformations before sinking. As particles are added, the raft grows, becomes denser, and lowers significantly, displacing a large amount

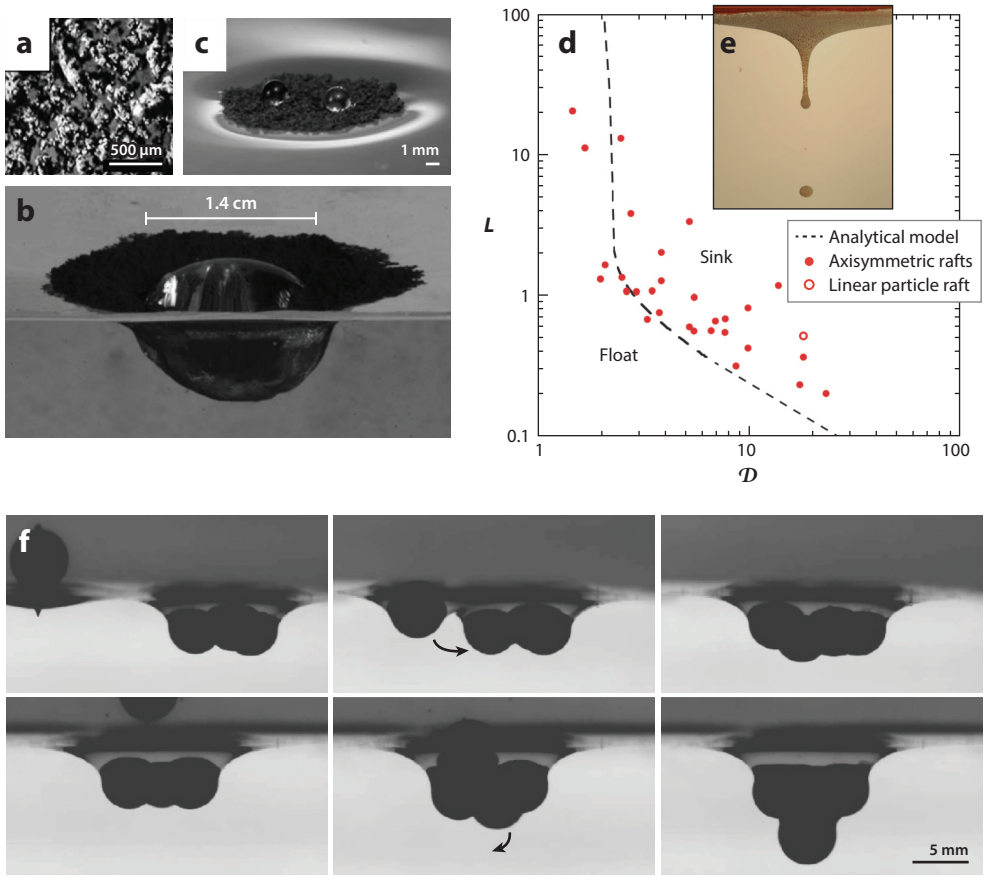

Figure 5

Sinking instability of a particle raft. (*a*) Surface of a particle raft made of superhydrophobic copper particles. (*b*) A water drop can create a large deformation in a sheet without sinking. (*c*) 1-mL drops on a superhydrophobic particle raft. (*d*) The transition between floating and sinking for axisymmetric particle rafts: the maximum arclength L of the raft before sinking as a function of the density ratio $\mathcal{D}$. The dashed line corresponds to the analytical model of the floating–sinking transition detailed by Protière et al. (2017). For small values of $\mathcal{D}$, a raft would never sink. The open red circle corresponds to a linear particle raft, whereas the other points correspond to axisymmetric rafts. (*e*) A raft at an oil–water interface; once unstable, it collapses by forming an oil jet with particles at its interface, which breaks further down into small armored droplets (droplet size ≈5 mm). (*f*) A sphere descending at the liquid–liquid interface, pulled toward an existing particle raft by capillary forces to finally self-assemble with the raft (*top*). A sphere descends from on top of the raft to rearrange within the raft and finally form a stack of particles that is out of equilibrium (*bottom*). Panels adapted with permission from (*a–c*) Larmour et al. (2008), copyright 2008 Wiley-VCH; (*d*) Protière et al. (2017), copyright 2017 American Physical Society; (*e*) Abkarian et al. (2013), copyright 2013 Nature; and (*f*) Jones et al. (2015), copyright 2015 AIP.

of liquid from under it. Similarly to Vella et al. (2006b), the authors reported that for $\mathcal{D} < 3$ a raft can grow infinitely large without sinking, as the hydrostatic pressure will always support its weight. However, for $\mathcal{D} > 3$, there always is a critical size at which the raft will collapse, as it would need to lower deeper than the capillary length in order to float, which surface tension does not permit; thus, the raft will sink (**Figure 5*d***).

We must note that the way the particles are deposited impacts the self-assembly of the objects at the liquid interface and plays a significant role in the limits of the overall system's stability. In particular, when particles are poured (Abkarian et al. 2013, Ong et al. 2019, Cervantes-Álvarez

et al. 2020) or stacked (Jones et al. 2015), they sink for a smaller number of particles than they do when they self-assemble in a monolayer (**Figure 5*f***). The specific configuration of the raft increases its potential load, as surface tension effects can increase with the raft size. For the same reason, a linear or axisymmetric raft will not sink for the same number of particles (**Figure 5*d***).

3.4. Beyond the Stability of a Particle Raft

Particle rafts are out of equilibrium once capillary forces cannot sustain their weight. They then start to collapse and sink. This destabilization process can also be triggered by applying a force on the raft or increasing its load. In particular, Larmour et al. (2008) studied how large floating rafts made of superhydrophobic copper particles can support objects that would normally sink (**Figure 5*a–c***). These sheets are flexible since they can deform when an object is placed on them, but they are robust enough that they do not tear or crack under loading. The sheet can then wrap heavy objects and the cohesion between the copper particles prohibits the penetration of liquid inside. Similarly, Jambon-Puillet et al. (2018) studied how centimetric drops can be placed on a particle raft and float on a bath of the same liquid. The raft is deformed by the load of the floating drop and the particles' weight, but it also prevents the coalescence of the drop with the liquid, as it acts as an armor. The raft can also be pushed down from above with a cylinder (Abkarian et al. 2013) to initiate its collapse in a controlled way: The particles slide down along the cylinder at a constant speed and thus sink continuously when reaching its tip.

When out of equilibrium, the raft then sinks below the interface. The dynamics of the sinking process is again linked to the dimensionless parameter $\mathcal{D}$. For large or dense particles ($\mathcal{D} > 3$ in **Figure 5*d***), the raft bows in the middle and encapsulates the upper liquid phase into a single large droplet as it sinks. For small or less dense particles ($\mathcal{D} < 3$ in **Figure 5*e***), as explained in the previous paragraph, the raft could be infinitely long and never sink. However, we have found that in this case, when rafts become several times longer than the capillary length, they can become metastable, as they are compressed by their own weight and wrinkles appear along the raft that grow and lead to total collapse (Protière et al. 2017, Guzowski & Gim 2019). The sinking process here is quite different, as one observes an interfacial granular jet that destabilizes due to a Rayleigh–Plateau-like instability and thus breaks down into millimeter-sized armored droplets, which we discuss in the last section of this review.

4. MECHANICAL PROPERTIES OF A PARTICLE RAFT

Several works have focused on investigating the mechanical properties of particle rafts. Contrary to suspensions, the particles form a 2D aggregate that is easy to visualize and probe. When subjected to various external stresses, it has been found that these aggregates undergo different types of structural changes (**Figure 6**), such as (*a*) rearrangements of the particles within the raft due to shear flows or low stresses that drive the particles to slide along one another; (*b*) free or controlled compression of the raft, which creates deformations that lead to its buckling; and (*c*) external flows that may force the particles to detach from the raft's rim and lead to its erosion or the breaking up of the raft into large pieces.

4.1. Rearrangements within a Particle Raft

At rest, a raft consisting of monodisperse particles will form a hexagonal lattice. Camoin & Blanc (1985) were the first to report an experimental study on 2D aggregates subjected to a shear, which they compared to the attractive capillary forces, and observed the formation of fractal structures. Whether in shear or extensional flow (Stancik et al. 2002, 2003) or subjected to Faraday surface waves (Sanlı et al. 2014), particles within a raft can rearrange. The particle concentrations or

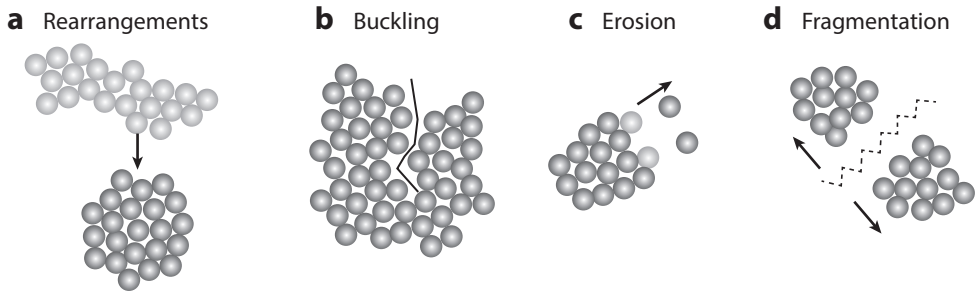

Figure 6

Possible changes in a particle raft subjected to an external force. (*a*) Reorganization of the internal structure. (*b*) Buckling of the raft, which induces the formation of cracks, wrinkles, or folds within the monolayer. (*c*) Erosion, in which a few particles can be pulled from the raft's rim. (*d*) Fragmentation, in which the raft breaks into various pieces of comparable sizes. Figure adapted with permission from Lagarde (2020), copyright 2020 the author.

surface area at the interface impacts the aggregate's structure (Berhanu & Kudrolli 2010). At low concentration (or high shear rates), particles may align in the flow direction and slide against each other, thus provoking a stretching of the aggregate. At high concentrations (or low shear rates), grain-to-grain interactions are strong and the particles are blocked in their lattice positions. In this case, domains within the cluster may rotate to accommodate the flow's direction. The force linked to rearrangements can be measured for a compressed 2D crystal made of monodisperse droplets (Ono-dit-Biot et al. 2020). It would be interesting to study the role of friction during rearrangements and compare those measurements to the controllable adhesion within 2D droplet crystals.

4.2. Buckling of a Particle Raft

A particle raft can also be compressed so as to increase its packing fraction in a controlled way (**Figure 7*a***). There comes a critical packing area where the particles cannot rearrange anymore: They are jammed. This creates a sudden global change of behavior where instead of observing in-plane motion within the raft such as small- or large-scale arrangements, we have a sudden out-of-plane deformation of the entire cluster and the raft starts to buckle. Similarly to surfactants at a liquid interface, this behavior can be quantified using a Langmuir trough equipped with Wilhelmy plates to measure the surface tension of the interface while the quantity of particles remains constant (Aveyard et al. 2000).

4.2.1. Elastic behavior. Once the interface has buckled, the particles are jammed and the raft reaches a transition from liquid-like to solid-like. Several works have focused on understanding this instability by considering the raft as a continuous elastic sheet floating at the surface of a fluid. The raft can then be characterized by its bending stiffness per unit width, $B = \frac{ER_{\text{part}}^3}{12(1-\nu^2)}$, with R_{part} the sheet thickness, ν the Poisson ratio, and a Young's modulus E, which depends on the characteristics of the interface (Vella et al. 2004). For large compressions, wrinkles are observed along the surface of the raft (**Figure 7*d*,*f***) at a characteristic wavelength λ. For an elastic sheet, we have

$$\lambda = 2\pi \left(\frac{B}{\Delta \rho g} \right)^{1/4}. \qquad 8.$$

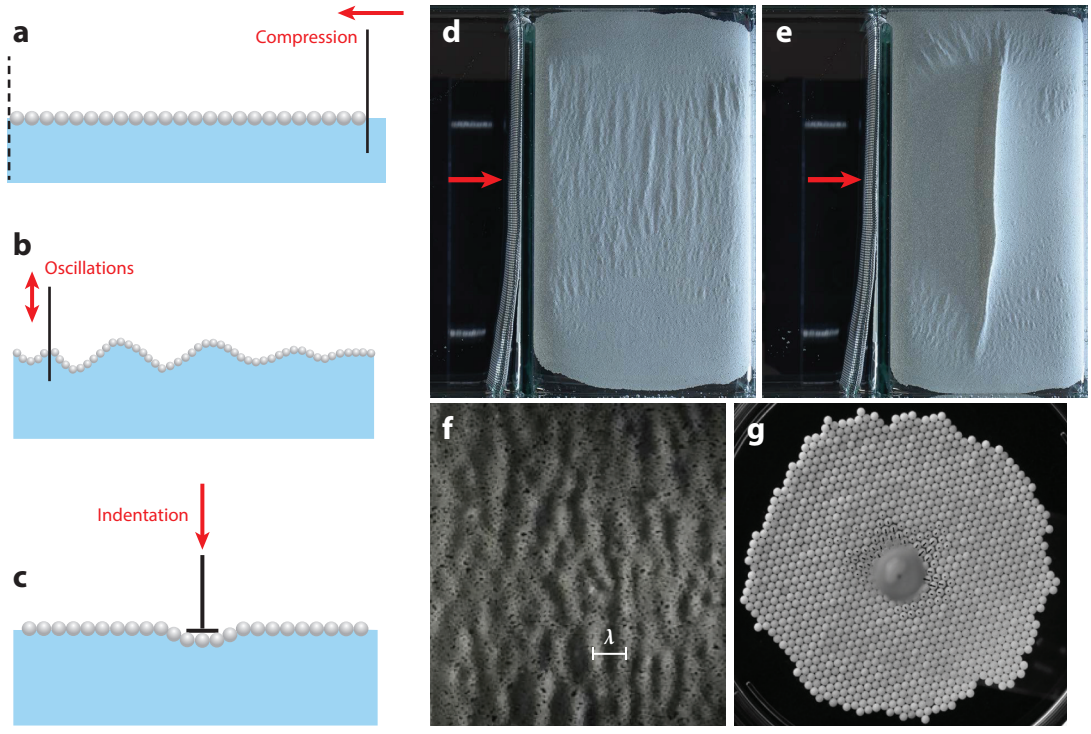

Figure 7

Various experimental setups to probe the mechanical properties of a particle raft, such as (*a*) compression, (*b*) oscillations to create surface waves, and (*c*) indentation. (*d*) By compressing a raft at an oil–water interface we observe wrinkles (view from below), which (*e*) localize into a single fold upon further compression (particle radius $R_{\text{part}} = 75$ μm). The arrows indicate the direction of compression. (*f*) Bottom view of a raft once it has buckled, which can be used to measure the wavelength λ of the wrinkles ($R_{\text{part}} = 250$ μm). (*g*) By poking a raft from above we observe particle rearrangements within the raft to accommodate the deformation. Panels adapted with permission from (*d–f*) Jambon-Puillet (2016), copyright 2016 the author, and (*g*) He et al. (2020), copyright 2020 Royal Society of Chemistry.

After measuring λ we can deduce an effective bending rigidity of the particle raft. With this 2D approach, Vella et al. (2004) considered the mean stress and strain within the raft and hypothesized that the strain only depends on the liquid surface area. They obtained an effective Young's modulus that depends on the 2D packing fraction ϕ:

$$E \sim \frac{(1-\nu)\gamma_{12}}{(1-\phi)R_{\text{part}}}, \qquad 9.$$

which we can substitute in Equation 8 to find

$$\lambda \sim \sqrt{\ell_c R_{\text{part}}}. \qquad 10.$$

Instead of compressing the raft, Planchette et al. (2012b) oscillated a plate orthogonally to its interface to excite surface waves on the particle-laden surface (**Figure 7*b***). They used a modified dispersion relation to include a bending term and the particles' inertia to characterize the raft's wave propagation. The authors proposed a model that takes into account the wettability of the particles via the contact angle θ (Kralchevsky et al. 2005); since the particles are adsorbed at the interface they have to move upward or downward to accommodate the pinning of the contact line.

Janssen effect: the weight of grains in a silo is distributed both vertically and laterally due to the transmission of forces between grains in contact; the latter is responsible for the collapse of the silo's walls, which are not built to resist such loads

This induces a variation of the free energy as a function of the interface's curvature. This model leads to the same relation for the bending rigidity that was deduced from the configuration of the particles within the raft under compression, $\lambda \sim \sqrt{R_{\text{part}}}$, with a prefactor that depends on the wetting properties of the particles. The term θ can be varied, but it does not modify the bending rigidity significantly enough to rule out the elastic sheet analogy.

Using both experimental techniques (compression or wave propagation), Petit et al. (2016) showed that the buckling of bidisperse particle rafts highlights the dual nature of the raft: Its elasticity is confirmed via collective effects and its granular character is also observed via the propagation of stresses through force chains. The limits of the analogy of a particle raft with a continuous elastic sheet have been tested with various experimental setups.

4.2.2. Granular characteristics. When further investigating the compression of rafts in a Langmuir trough, Cicuta & Vella (2009) have shown that by orienting the Wilhelmy plates parallel or orthogonal to the moving barriers, the critical buckling pressure will vary. The exponential decay for the surface pressure is then explained by arguing that the stress propagates through force chains and the walls absorb part of the stress, similarly to the Janssen effect observed in 3D granular silos (Janssen 1895). The role of friction is also discussed by Saavedra et al. (2018), who distributed flexible pressure sensors along the raft and measured the gradual development of internal stresses within the raft. They found that the screening of the pressure stress is much stronger and may be due to localized compaction effects. Similarly, local plastic instabilities are linked to a weakening of the shear response during the jamming transition (Varshney et al. 2012) and attributed to a local depinning of the contact line.

Most studies have focused on small deformations, in which the onset of buckling of the raft is linked to frictional forces once the particles have reached the jamming concentration. This elastic behavior can be studied in a controlled way by compressing these rafts beyond wrinkling. Jambon-Puillet et al. (2017) pushed this analogy even further by checking experimentally whether it is still valid for large deformations. They investigated the buckling instability in the compression of granular rafts in the linear and nonlinear regimes. In this case, a second wavelength of wrinkles was measured [which was also observed by Kassuga & Rothstein (2015)], and at larger compression, they observed the localization of the wrinkles into a single fold that grows until the entire raft sinks (**Figure 7*d*,*e***). This is reminiscent of the reversible wrinkle-to-fold transition observed for a floating elastic sheet. After further probing of the limits of a continuum elastic model, it was found that the granular raft exhibits specific mechanical properties, in particular, an irreversible plastic transition, which is observed in hysteretic behavior during compression cycles. When the particles are stirred, forcing new random particle arrangements, networks of intense force chains may be broken and the raft can recover its elastic properties. The raft's dual nature—granular and elastic—is thus highlighted during this process.

By locally indenting the raft (**Figure 7*c***), researchers can probe the elastic response of a particle raft to normal forces as well (Zuo et al. 2017, He et al. 2020). For thin elastic sheets, wrinkles extend radially outward from the indentation, but for rafts, particles can rearrange, and their motions away from the indentation allow the lattice to accommodate the azimuthal compression without leading to a buckling instability, which shows that the raft behaves as a fluid interface (**Figure 7*g***). The raft can also withstand large indentation depths, act as a mechanical protection to the interface, and enable the production of armored droplets of controlled volume and particle coverage (Abkarian et al. 2013). A body force such as a magnetic field can also be used to induce an upward bending of the raft, and the forces needed to create a deformation can then be quantitatively measured from the magnetic forces (Zuo et al. 2021).

4.3. Testing the Cohesion of a Particle Raft: Erosion, Fractures, and Fragmentation

When an external flow is applied to a capillary raft, single particles can detach from the parent raft's edges. We call this process surface erosion. The raft remains mostly intact except for a few particles lost at its edges (Lagarde & Protière 2020). When the raft breaks up into larger pieces, we have a fragmentation of the raft. Studying how and where aggregates break allows researchers to test the cohesion of a raft and investigate the interparticle interactions within it. Vassileva et al. (2007) discussed the critical shear rate for breakup by erosion or fragmentation. In particular, they found that the two processes occur at different shear rates, as the normal forces in the center of the aggregate are larger than those near its rim. Moreover, the critical shear rate depends weakly on the aggregate size of the raft and the particles' radii. Since friction forces are larger for large particles (due to a larger grain-to-grain contact), large particle aggregates will hardly rearrange, while a small defect may induce crack growth and further fracturing; in contrast, for smaller particles, erosion is possible. One model based on the balance between the viscous drag, which creates deformations that facilitate the breaking up of the raft, and the attractive capillary forces that bind the particles into an aggregate predicts the cluster size distribution in a shear flow (Huang et al. 2012).

Another way to test the cohesion of a raft is to apply a radial stress. Kim et al. (2019) proposed an experimental method where a densely packed raft is placed in a funnel and the water level is progressively raised. In this case, depending on the intensity of the attractive force between the particles (which they controlled by varying their density), the raft will fracture or the particles will move and rearrange to heal small fractures. By performing quasi-static tensile tests on a particle raft, Xiao et al. (2020) observed similar plastic rearrangements and failures. The ductility of the material can be tuned by varying the interaction range for the capillary attractions. Large particles interact at shorter distances; for example, the rafts then fracture at small tensile deformations, leading to brittle behavior. In contrast, rafts made of small particles have long-ranged interactions and can rearrange more easily; by preventing any eventual voids from growing, they show less brittle behavior. Fractures are also observed when locally adding a surfactant at the center of a raft (Vella et al. 2006a). In this case, the crack propagation is mostly due to the advection of surfactant toward the crack tip, but its branching seems mostly due to the raft's solid-like response. When impacting a droplet on the surface of the particle raft, Planchette et al. (2018) observed that the mechanisms leading to its rupture and robustness are based on the size distribution of its particles as collective effects become apparent. These results confirm the importance of the steric repulsion between the particles in the solid-like response of particle rafts.

5. ARMORED DROPLETS

In this section, we describe a few results detailing the mechanical properties of armored droplets (i.e., liquid droplets adorned with a monolayer of particles adsorbed at their curved surfaces). With such systems, the mechanical properties of particle-laden drop surfaces can be investigated via various experimental configurations.

As we have detailed in the previous section, the jamming of a particle-laden interface occurs when the particle concentration at the interface increases (or, conversely, when the surface area decreases). Shrinking the volume of armored droplets is a common method to reduce their interfacial area and force the compaction of the particles at their surfaces. This phenomenon leads to a similar solid-like behavior discussed above for rafts, with wrinkles appearing at the surface of the droplet (Monteux et al. 2007). With this protective shell, coalescence, which would increase surface area and therefore lead to less stable droplets, is also inhibited. To modify the

armored droplet's volume, one can progressively remove the bulk liquid and simultaneously measure its internal pressure ΔP. Alternatively, one can quasi-statically compress the shell by slowly evaporating the droplet, thereby keeping the boundary conditions intact, and image the droplet shape and granular interface to measure the variation of the solid fraction and the drop's effective surface tension (Lagubeau et al. 2014). At first, the armored droplet's pressure corresponds to the Laplace pressure $2\gamma_{12}/R$ (with R the droplet radius and γ_{12} the interfacial tension), but then it decreases drastically to 0 due to the collapse of the droplet as jamming occurs, the particles' interactions make the pressure drop, and the surface starts to wrinkle. This critical collapse pressure P_c can be compared to the behavior of the collapse of a solid spherical shell using various physical models (Pitois et al. 2015, Taccoen et al. 2016, Pitois & Rouyer 2019). Similar observations have been made for armored bubbles where, interestingly, jamming particles at their liquid–gas interface can extend their lifetimes indefinitely (Pitois & Rouyer 2019).

Armored droplets with jammed particles at their surfaces can be squeezed mechanically (Rendos et al. 2017) or can rupture upon impact (Aussillous & Quéré 2006, Planchette et al. 2012a). These two methods probe the droplets' robustness directly or indirectly (Ji et al. 2020). These large deformations lead to fracturing of the shell. Indeed, upon impact at a critical velocity, an armored droplet spreads on the solid substrate and thus increases its surface area. This creates a hole in the armor, which can then wet the solid surface in this region. The armored droplet will adhere to the surface at this point, and its integrity is lost. The rupture mechanism is still unknown but seems to depend on the particle size: A single crack is observed for small particles and multiple holes are observed for larger particles, which shows that interparticle forces play an important role here (**Figure 8*a***).

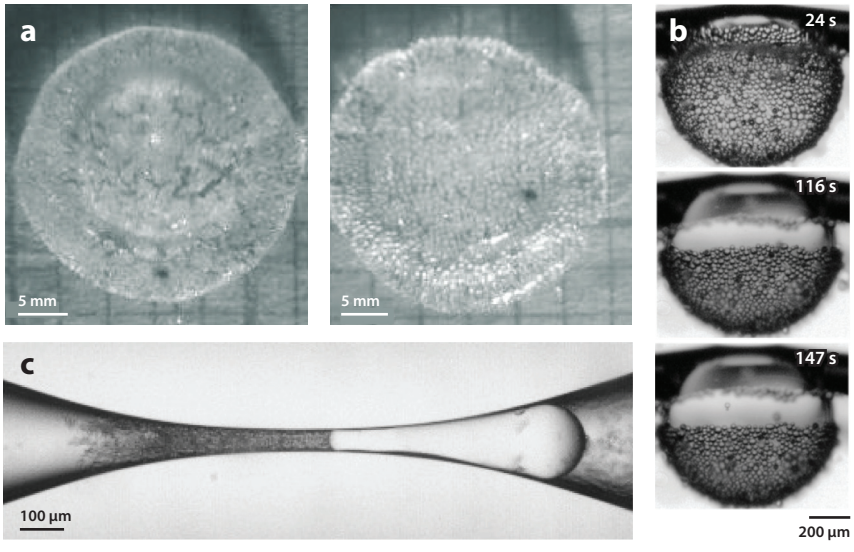

Figure 8

Particle-laden interfaces can lose their integrity. (*a*) When subjected to a large deformation such as an impact, an armored droplet will fracture its shell. Here we see the top view of the impacts, with particle radius $R_{part} = 16$ m (*left*) and $R_{part} = 67$ µm (*right*). (*b*) An armored droplet destabilized by gravity sheds particles until reaching an equilibrium between buoyancy and weight. (*c*) An armored droplet flowing through a constriction will eject particles at large flow rates. Panels adapted with permission from (*a*) Planchette et al. (2012a), copyright 2012 EPLA; (*b*) Tavacoli et al. (2012), copyright 2012 American Physical Society; and (*c*) de Soëte (2021), copyright 2021 the author.

Thus far, we have discussed the particular case of liquid marbles or armored bubbles that are formed at an air–water interface. However, the stability of emulsions is known to be enhanced by adding hydrophobic solid particles at the oil–water interface since the pioneering work of Pickering (1907). Since then, so-called Pickering emulsions have been investigated thoroughly for many applications (Binks & Lumsdon 2001, Binks & Horozov 2006). These particles can be coupled to external fields in order to control their stability and capture or release the liquid inside the capsule. Interestingly, when the density of the particles is larger than the density of the outer liquid, $\rho_{\text{part}} > \rho_1$, oil-in-water armored droplets can be destabilized by gravity (Tavacoli et al. 2012). This process is entirely governed by a modified Bond number, which here compares the external force on one particle, namely gravity, to the maximal capillary force that keeps it adsorbed to the interface: $\mathcal{B}o = (R_{\text{part}}/\ell_c)^2$. The limiting droplet size for these buoyant armored droplets under gravity is therefore $D_{\max} = \ell_c$, or the maximum number of particles N_m that can be trapped at the surface of the droplet: $D_{\max} = \sqrt{N_m} R_{\text{part}}$ (**Figure 8*b***). Above this threshold, particles are ejected. This limit takes into account the characteristics of the two liquid phases but does not account for variations in the particles' densities. Abkarian et al. (2013) highlighted the role of the particles by studying highly dense particles adsorbed at the oil–water interface of centimetric droplets. In this case, by adding oil progressively to such armored droplets, their buoyancy increases and it is the particles' weight that contains the oil and prevents it from escaping the droplet. For a critical oil volume, destabilization occurs via two scenarios depending on the parameters of the experiments: The entire droplet can become buoyant and float to the surface, or the uncovered portion of the droplet can pinch off, leaving behind a small armored droplet.

These armored droplets have been further investigated beyond buckling when subjected to large deformations. In particular, curvature effects can lead to particle desorption instead of buckling when the surface pressure increases for large values of R_{part}/R (Gu & Botto 2018, Guzowski & Gim 2019). Armored droplets undergo strong deformations when placed in an extensional flow or a constriction, or during extremely fast events such as their coalescence or the oscillations due to an acoustic field (Garbin 2019, de Soëte 2021). These dynamic phenomena also lead to the ejection of particles (via a rapid expulsion or a slow shedding), which is a topic that has only recently been explored (**Figure 8*c***).

SUMMARY POINTS

1. Non-Brownian particles present at a liquid–liquid interface create local deformations that induce long-ranged attractive capillary interactions among objects that self-assemble into a capillary raft: a monolayer of grains. The clustering dynamics depends on the number of particles within the clusters.
2. Although individual particles within a raft float independently thanks to Archimedes' Principle, the entire particle assembly can become unstable and sink in the case of large flotation forces. The critical shape of the capillary raft depends on a modified Bond number, which takes into account the characteristics of the particles and the liquid.
3. The mechanical properties of a particle raft have been probed by subjecting it to various external stresses. It behaves as a single entity and can be modeled as a continuous elastic sheet, as wrinkles and folds can be observed when it is compressed, but its discrete nature is also responsible for restructuring within the raft or plastic deformations due to interparticle interactions.

4. The integrity of droplets coated by a protective armor of jammed particles, or so-called armored droplets, has been examined via various methods. In particular, armored droplets are found to fracture or eject particles when subjected to large deformations. The stability of the armor, as well as the cohesion between the individual particles, is then lost.

FUTURE ISSUES

1. We still lack a complete model for the clustering dynamics of dispersed particles into a single granular raft where the role of gravity and the additivity are fully described. In this case, objects form clusters with their closest neighbors but will eventually merge with the largest raft due to its strong attractive potential. The clustering process therefore depends on the rate of creation of a given raft compared to its aggregation with other clusters, which is uncommon in the clustering dynamics of passive systems.
2. A particle raft's cohesion is due to the attractive capillary interactions between the grains. The plastic behavior of a granular raft, however, occurs when the particles come into contact. This implies that friction between the grains plays an important role beyond the jamming transition. Bridging the liquid and granular aspects of particle rafts by controlling the friction coefficient, for example, would allow us to describe the plastic transition observed beyond the elastic analogy and fully describe the composite nature of this material. We are still lacking a full granular and elastic model that would include the wrinkling and bending of the raft under compression.
3. Large deformations of armored droplets or granular rafts have been observed when subjected to external body forces, external fields, or various types of flows. They lead to new types of behavior, such as the expulsion of particles or the dynamic collapse of the raft. Investigating these dynamic effects will improve our current knowledge of the mechanics of these composite materials in realistic conditions.
4. Similarly, measurements of the forces needed to break up or fragment a particle raft are still scarce and would offer a different insight into the cohesion of its structure. Moreover, the role of defects during the fragmentation process is still unclear. Once we understand a raft's disassembly we could then create or break large structures whose microstructures could rearrange at interfaces.
5. Until now, we have only discussed the self-assembly of passive particles at interfaces. The study of how clusters of active particles behave when confined to interfaces is now an emerging field. Active particles driven by an external field (oriented by surface curvature or another body force, for example) or with their own inertia will potentially affect their collective behavior and directed self-assembly.
6. The two fluids creating the interface at which the particles self-assemble into a particle raft are always Newtonian, with properties that do not vary depending on the dynamics. Particle rafts can undergo fast deformations or rapid collapses. At complex fluid interfaces, one could expect these processes, as well as the mechanical properties of the particle raft, to be greatly affected and thus completely change their overall behavior.

DISCLOSURE STATEMENT

The author is not aware of any biases that might be perceived as affecting the objectivity of this review.

ACKNOWLEDGMENTS

I am particularly grateful to Antoine Lagarde and Etienne-Jambon Puillet, with whom I have shared many insightful conversations. It is also my pleasure to thank Christophe Josserand and Manouk Abkarian for stimulating discussions and Matthieu Roché for encouragements. This work was supported by the Sorbonne Université Emergence program.

LITERATURE CITED

Abkarian M, Protière S, Aristoff JM, Stone HA. 2013. Gravity-induced encapsulation of liquids by destabilization of granular rafts. *Nat. Commun.* 4:1895

Allain C, Cloitre M. 1993. Interaction between particles trapped at fluid interfaces: I. Exact and asymptotic solutions for the force between two horizontal cylinders. *J. Colloid Interface Sci.* 157(2):261–68

Aussillous P, Quéré D. 2006. Properties of liquid marbles. *Proc. R. Soc. A* 462(2067):973–99

Aveyard R, Clint JH, Nees D, Quirke N. 2000. Structure and collapse of particle monolayers under lateral pressure at the octane/aqueous surfactant solution interface. *Langmuir* 16(23):8820–28

Batchelor G. 1976. Brownian diffusion of particles with hydrodynamic interaction. *J. Fluid Mech.* 74(1):1–29

Batchelor G, Green JT. 1972. The hydrodynamic interaction of two small freely-moving spheres in a linear flow field. *J. Fluid Mech.* 56(2):375–400

Berhanu M, Kudrolli A. 2010. Heterogeneous structure of granular aggregates with capillary interactions. *Phys. Rev. Lett.* 105(9):098002

Binks BP, Horozov TS. 2006. *Colloidal Particles at Liquid Interfaces*. Cambridge, UK: Cambridge Univ. Press

Binks BP, Lumsdon S. 2001. Pickering emulsions stabilized by monodisperse latex particles: effects of particle size. *Langmuir* 17(15):4540–47

Bleibel J, Dietrich S, Domìnguez A, Oettel M. 2011. Shock waves in capillary collapse of colloids: a model system for screened Newtonian gravity. *Phys. Rev. Lett.* 107:128302

Boneva MP, Christov NC, Danov KD, Kralchevsky PA. 2007. Effect of electric-field-induced capillary attraction on the motion of particles at an oil–water interface. *Phys. Chem. Chem. Phys.* 9(48):6371–84

Bowden N, Terfort A, Carbeck J, Whitesides GM. 1997. Self-assembly of mesoscale objects into ordered two-dimensional arrays. *Science* 276(5310):233–35

Camoin C, Blanc R. 1985. Aggregation in a sheared 2D dispersion of spheres with attractive interactions. *J. Phys. Lett.* 46(2):67–74

Cavallaro M, Botto L, Lewandowski EP, Wang M, Stebe KJ. 2011. Curvature-driven capillary migration and assembly of rod-like particles. *PNAS* 108(52):20923–28

Cervantes-Álvarez A, Escobar-Ortega Y, Sauret A, Pacheco-Vázquez F. 2020. Air entrainment and granular bubbles generated by a jet of grains entering water. *J. Colloid Interface Sci.* 574:285–92

Chan D, Henry J, White L. 1981. The interaction of colloidal particles collected at fluid interfaces. *J. Colloid Interface Sci.* 79(2):410–18

Cicuta P, Vella D. 2009. Granular character of particle rafts. *Phys. Rev. Lett.* 102(13):138302

Cooray H, Cicuta P, Vella D. 2017. Floating and sinking of a pair of spheres at a liquid–fluid interface. *Langmuir* 33(6):1427–36

Cózar A, Echevarra F, González-Gordillo JI, Irigoien X, Úbeda B, et al. 2014. Plastic debris in the open ocean. *PNAS* 111(28):10239–44

Dalbe MJ, Cosic D, Berhanu M, Kudrolli A. 2011. Aggregation of frictional particles due to capillary attraction. *Phys. Rev. E* 83(5):051403

Dani A, Keiser G, Yeganeh M, Maldarelli C. 2015. Hydrodynamics of particles at an oil–water interface. *Langmuir* 31(49):13290–302

Danov KD, Aust R, Durst F, Lange U. 1995. Influence of the surface viscosity on the hydrodynamic resistance and surface diffusivity of a large Brownian particle. *J. Colloid Interface Sci.* 175(1):36–45

Danov KD, Dimova R, Pouligny B. 2000. Viscous drag of a solid sphere straddling a spherical or flat surface. *Phys. Fluids* 12(11):2711–22

Danov KD, Kralchevsky PA, Naydenov BN, Brenn G. 2005. Interactions between particles with an undulated contact line at a fluid interface: capillary multipoles of arbitrary order. *J. Colloid Interface Sci.* 287(1):121–34

de Soëte F. 2021. *Ecoulement de gouttes couvertes dans une contraction*. PhD Thesis, Univ. PSL, Paris

Domìnguez A, Oettel M, Dietrich S. 2010. Dynamics of colloidal particles with capillary interactions. *Phys. Rev. E* 82:011402

Fournier JB, Galatola P. 2002. Anisotropic capillary interactions and jamming of colloidal particles trapped at a liquid-fluid interface. *Phys. Rev. E* 65(3):031601

Friedlander SK. 2000. *Smoke, Dust, and Haze*. New York: Oxford Univ. Press

Garbin V. 2019. Collapse mechanisms and extreme deformation of particle-laden interfaces. *Curr. Opin. Colloid Interface Sci.* 39:202–11

Gifford W, Scriven L. 1971. On the attraction of floating particles. *Chem. Eng. Sci.* 26(3):287–97

Grzybowski BA, Stone HA, Whitesides GM. 2000. Dynamic self-assembly of magnetized, millimetre-sized objects rotating at a liquid–air interface. *Nature* 405(6790):1033–36

Gu C, Botto L. 2018. Buckling vs. particle desorption in a particle-covered drop subject to compressive surface stresses: a simulation study. *Soft Matter* 14(5):711–24

Guzowski J, Gim B. 2019. Particle clusters at fluid–fluid interfaces: equilibrium profiles, structural mechanics and stability against detachment. *Soft Matter* 15(24):4921–38

He W, Sun Y, Dinsmore AD. 2020. Response of a raft of particles to a local indentation. *Soft Matter* 16(10):2497–505

Hornbaker D, Albert R, Albert I, Barabási AL, Schiffer P. 1997. What keeps sandcastles standing? *Nature* 387(6635):765–65

Hu Z, Fang W, Li Q, Feng XQ, Lv Ja. 2020. Optocapillarity-driven assembly and reconfiguration of liquid crystal polymer actuators. *Nat. Commun.* 11:5780

Huang K, Brinkmann M, Herminghaus S. 2012. Wet granular rafts: aggregation in two dimensions under shear flow. *Soft Matter* 8(47):11939–48

Jambon-Puillet E. 2016. *Folds in floating membranes: from elastic sheets to granular rafts*. PhD Thesis, Univ. Pierre Marie Curie, Sorbonne Univ., Inst. Jean le Rond d'Alembert, Paris

Jambon-Puillet E, Josserand C, Protière S. 2017. Wrinkles, folds, and plasticity in granular rafts. *Phys. Rev. Mater.* 1(4):042601

Jambon-Puillet E, Josserand C, Protière S. 2018. Drops floating on granular rafts: a tool for liquid transport and delivery. *Langmuir* 34(15):4437–44

Janssen HA. 1895. Versuche über Getreidedruck in Silozellen. *Z. Ver. dtsch. Ing.* 39:1045–49

Ji X, Wang X, Zhang Y, Zang D. 2020. Interfacial viscoelasticity and jamming of colloidal particles at fluid–fluid interfaces: a review. *Rep. Prog. Phys.* 83(12):126601

Jones SG, Abbasi N, Ahuja A, Truong V, Tsai SSH. 2015. Floating and sinking of self-assembled spheres on liquid-liquid interfaces: rafts versus stacks. *Phys. Fluids* 27(7):072102

Kassuga TD, Rothstein JP. 2015. Buckling of particle-laden interfaces. *J. Colloid Interface Sci.* 448:287–96

Keller JB. 1998. Surface tension force on a partly submerged body. *Phys. Fluids* 10(11):3009–10

Kim BL, Rendos A, Ganesh P, Brown KA. 2019. Failure of particle-laden interfaces studied using the funnel method. *Colloid Interface Sci. Commun.* 28:54–59

Kralchevsky PA, Denkov ND. 2001. Capillary forces and structuring in layers of colloid particles. *Curr. Opin. Colloid Interface Sci.* 6(4):383–401

Kralchevsky PA, Ivanov IB, Ananthapadmanabhan KP, Lips A. 2005. On the thermodynamics of particle-stabilized emulsions: curvature effects and catastrophic phase inversion. *Langmuir* 21(1):50–63

Kralchevsky PA, Nagayama K. 1994. Capillary forces between colloidal particles. *Langmuir* 10(1):23–36

Kralchevsky PA, Nagayama K. 2001. Capillary bridges and capillary-bridge forces. In *Studies in Interface Science*, vol. 10, pp. 469–502. Amsterdam: Elsevier

Kralchevsky PA, Paunov V, Ivanov I, Nagayama K. 1992. Capillary meniscus interaction between colloidal particles attached to a liquid–fluid interface. *J. Colloid Interface Sci.* 151(1):79–94
Lagarde A. 2020. *Folds in floating membranes: from elastic sheets to granular rafts*. PhD Thesis, Sorbonne Univ., Inst. Jean le Rond d'Alembert, Paris
Lagarde A, Josserand C, Protière S. 2019. The capillary interaction between pairs of granular rafts. *Soft Matter* 15(28):5695–702
Lagarde A, Protière S. 2020. Probing the erosion and cohesion of a granular raft in motion. *Phys. Rev. Fluids* 5(4):044003
Lagubeau G, Rescaglio A, Melo F. 2014. Armoring a droplet: soft jamming of a dense granular interface. *Phys. Rev. E* 90(3):030201
Larmour IA, Saunders GC, Bell SEJ. 2008. Sheets of large superhydrophobic metal particles self assembled on water by the Cheerios effect. *Angew. Chem. Int. Ed.* 47(27):5043–45
Lee MH. 2000. On the validity of the coagulation equation and the nature of runaway growth. *Icarus* 143(1):74–86
Lehmann P, Aminzadeh M, Or D. 2019. Evaporation suppression from water bodies using floating covers: laboratory studies of cover type, wind, and radiation effects. *Water Resour. Res.* 55(6):4839–53
Leyvraz F. 2003. Scaling theory and exactly solved models in the kinetics of irreversible aggregation. *Phys. Rep.* 383(2–3):95–212
Lin M, Lindsay H, Weitz D, Ball R, Klein R, Meakin P. 1989. Universality in colloid aggregation. *Nature* 339(6223):360–62
Liu IB, Sharifi-Mood N, Stebe KJ. 2018. Capillary assembly of colloids: interactions on planar and curved interfaces. *Annu. Rev. Condensed Matter Phys.* 9:283–305
Loudet JC, Alsayed AM, Zhang J, Yodh AG. 2005. Capillary interactions between anisotropic colloidal particles. *Phys. Rev. Lett.* 94(1):018301
Loudet JC, Pouligny B. 2011. How do mosquito eggs self-assemble on the water surface? *Eur. Phys. J. E* 34(8):76
Mlot NJ, Tovey CA, Hu DL. 2011. Fire ants self-assemble into waterproof rafts to survive floods. *PNAS* 108(19):7669–73
Monteux C, Kirkwood J, Xu H, Jung E, Fuller GG. 2007. Determining the mechanical response of particle-laden fluid interfaces using surface pressure isotherms and bulk pressure measurements of droplets. *Phys. Chem. Chem. Phys.* 9(48):6344–50
Nicolson MM. 1949. The interaction between floating particles. *Proc. Camb. Philos. Soc.* 45(2):288–95
Ong XY, Taylor SE, Ramaioli M. 2019. Pouring of grains onto liquid surfaces: dispersion or lump formation? *Langmuir* 35(34):11150–56
Ono-dit-Biot JC, Soulard P, Barkley S, Weeks ER, Salez T, et al. 2020. Rearrangement of two dimensional aggregates of droplets under compression: signatures of the energy landscape from crystal to glass. *Phys. Rev. Res.* 2(2):023070
Paunov V, Kralchevsky P, Denkov N, Nagayama K. 1993. Lateral capillary forces between floating submillimeter particles. *J. Colloid Interface Sci.* 157(1):100–12
Petit P, Biance AL, Lorenceau E, Planchette C. 2016. Bending modulus of bidisperse particle rafts: local and collective contributions. *Phys. Rev. E* 93(4):042802
Pickering SU. 1907. Emulsions. *J. Chem. Soc.* 91:2001–21
Pitois O, Buisson M, Chateau X. 2015. On the collapse pressure of armored bubbles and drops. *Eur. Phys. J. E* 38(5):48
Pitois O, Rouyer F. 2019. Rheology of particulate rafts, films, and foams. *Curr. Opin. Colloid Interface Sci.* 43:125–37
Planchette C, Biance AL, Lorenceau E. 2012a. Transition of liquid marble impacts onto solid surfaces. *EPL* 97(1):14003
Planchette C, Lorenceau E, Biance AL. 2012b. Surface wave on a particle raft. *Soft Matter* 8(8):2444–51
Planchette C, Lorenceau E, Biance AL. 2018. Rupture of granular rafts: effects of particle mobility and polydispersity. *Soft Matter* 14(31):6419–30
Pozrikidis C. 2007. Particle motion near and inside an interface. *J. Fluid Mech.* 575:333–57
Protière S, Josserand C, Aristoff JM, Stone HA, Abkarian M. 2017. Sinking a granular raft. *Phys. Rev. Lett.* 118(10):108001

Rendos A, Alsharif N, Kim BL, Brown KA. 2017. Elasticity and failure of liquid marbles: influence of particle coating and marble volume. *Soft Matter* 13(47):8903–9

Saavedra OV, Elettro H, Melo F. 2018. Progressive friction mobilization and enhanced Janssen's screening in confined granular rafts. *Phys. Rev. Mater.* 2(4):043603

Sanlı C, Saitoh K, Luding S, van der Meer D. 2014. Collective motion of macroscopic spheres floating on capillary ripples: dynamic heterogeneity and dynamic criticality. *Phys. Rev. E* 90(3):033018

Stamou D, Duschl C, Johannsmann D. 2000. Long-range attraction between colloidal spheres at the air-water interface: the consequence of an irregular meniscus. *Phys. Rev. E* 62(4):5263–72

Stancik EJ, Gavranovic GT, Widenbrant MJ, Laschitsch AT, Vermant J, Fuller GG. 2003. Structure and dynamics of particle monolayers at a liquid–liquid interface subjected to shear flow. *Faraday Discuss.* 123:145–56

Stancik EJ, Widenbrant MJ, Laschitsch AT, Vermant J, Fuller GG. 2002. Structure and dynamics of particle monolayers at a liquid–liquid interface subjected to extensional flow. *Langmuir* 18(11):4372–75

Taccoen N, Lequeux FMC, Gunes DZ, Baroud CN. 2016. Probing the mechanical strength of an armored bubble and its implication to particle-stabilized foams. *Phys. Rev. X* 6(1):011010

Tavacoli JW, Katgert G, Kim EG, Cates ME, Clegg PS. 2012. Size limit for particle-stabilized emulsion droplets under gravity. *Phys. Rev. Lett.* 108(26):268306

Vandewalle N, Poty M, Vanesse N, Caprasse J, Defize T, Jérôme C. 2020. Switchable self-assembled capillary structures. *Soft Matter* 16(45):10320–25

Varshney A, Sane A, Ghosh S, Bhattacharya S. 2012. Amorphous to amorphous transition in particle rafts. *Phys. Rev. E* 86(3):031402

Vassileva ND, van den Ende D, Mugele F, Mellema J. 2005. Capillary forces between spherical particles floating at a liquid–liquid interface. *Langmuir* 21(24):11190–200

Vassileva ND, van den Ende D, Mugele F, Mellema J. 2006. Restructuring and break-up of two-dimensional aggregates in shear flow. *Langmuir* 22(11):4959–67

Vassileva ND, van den Ende D, Mugele F, Mellema J. 2007. Fragmentation and erosion of two-dimensional aggregates in shear flow. *Langmuir* 23(5):2352–61

Vella D. 2015. Floating versus sinking. *Annu. Rev. Fluid Mech.* 47:115–35

Vella D, Aussillous P, Mahadevan L. 2004. Elasticity of an interfacial particle raft. *EPL* 68(2):212

Vella D, Kim HY, Aussillous P, Mahadevan L. 2006a. Dynamics of surfactant-driven fracture of particle rafts. *Phys. Rev. Lett.* 96(17):178301

Vella D, Mahadevan L. 2005. The "Cheerios effect." *Am. J. Phys.* 73(9):817–25

Vella D, Metcalfe PD, Whittaker RJ. 2006b. Equilibrium conditions for the floating of multiple interfacial objects. *J. Fluid Mech.* 549:215–24

Voise J, Schindler M, Casas J, Raphaël E. 2011. Capillary-based static self-assembly in higher organisms. *J. R. Soc. Interface* 8(62):1357–66

Wang W, Giltinan J, Zakharchenko S, Sitti M. 2017. Dynamic and programmable self-assembly of micro-rafts at the air-water interface. *Sci. Adv.* 3(5):e1602522

Weitz D, Lin M. 1986. Dynamic scaling of cluster-mass distributions in kinetic colloid aggregation. *Phys. Rev. Lett.* 57(16):2037–40

Xiao H, Ivancic RJS, Durian DJ. 2020. Strain localization and failure of disordered particle rafts with tunable ductility during tensile deformation. *Soft Matter* 16(35):8226–36

Zuo P, Cheng Y, Wang Z, Dou X, Liu J. 2021. Tension and bending of the particle raft driven by a magnet. *Colloid Interface Sci. Commun.* 45:100528

Zuo P, Liu J, Li S. 2017. The load-bearing ability of a particle raft under the transverse compression of a slender rod. *Soft Matter* 13(12):2315–21